

Chapter 3

Technical Aspects of Scanning Probe Microscopy

3.1 Piezoelectric Effect

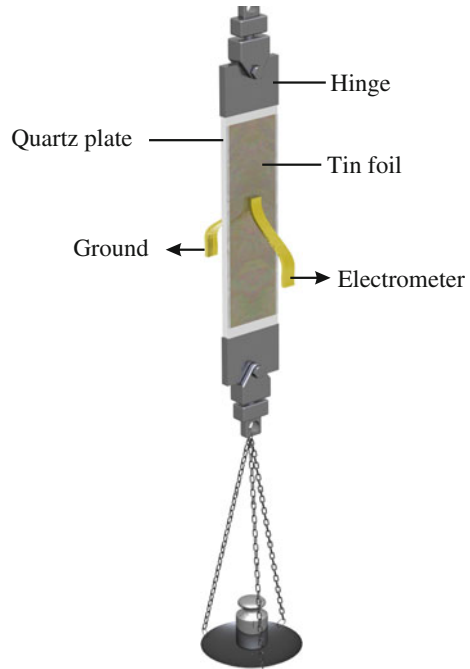
In order to position the probe tip or the sample, piezoelectric elements are used as actuators. The piezoelectric effect was discovered by the Curie brothers in 1880. A sketch of their experiment is shown in Fig. 3.1. Tin foils were attached as electrodes to two sides of a quartz plate. One tin foil was grounded and one connected to an electrometer. While a force was applied to generate vertical strain, an electrical charge was detected by the electrometer. The piezoelectric effect is used, for instance, to ignite pocket lighters (generating the voltage which generates the lightning spark) and many other technical applications such as sensor technology.

The converse effect occurs if a variable voltage is applied to the foils and a deformation of the crystal results. The converse piezoelectric effect is used in piezoelectric actuators. Since this deformation is very small and a continuous quantity, deformations much smaller than the diameter of an atom can be obtained for reasonably small voltages in the mV range.

In order to apply an external electric field inside the (electrically insulating) piezoelectric material, metallic electrodes at the surface are used. A voltage applied to the electrodes induces an electric field in the piezo material (as in a capacitor with a dielectric) and finally results in an extension of the piezo material. Vice versa, a strain of the piezo material leads to a surface charge and thus to a charge on the electrodes, and finally to a voltage between the electrodes.

The piezoelectric effect occurs only for crystals which are not centrosymmetric, i.e. do not have an inversion center. If an inversion center exists no net electric dipole moment can be induced inside the unit cell by straining the crystal. If a dipole moment is present at a position \mathbf{r} inside the unit cell, the opposite dipole is also present at the position $-\mathbf{r}$ due to the inversion symmetry and the net dipole moment of the unit cell is zero. During a directional deformation of a piezoelectric material, microscopic dipoles are formed inside the crystallographic unit cell. These microscopic dipoles lead to a charge at the surface of the crystal and a corresponding electric field inside the crystal. In the converse piezoelectric effect, the crystal unit cell is deformed by an

Fig. 3.1 Curie brothers' experiment demonstrating the piezoelectric effect



external applied electrical field. An example of a piezoelectric material is crystalline quartz. Another example of a piezoelectric material used in piezoelectric actuators is PZT ceramics (lead zirconate titanate $\text{Pb}[\text{Zr}_x\text{Ti}_{1-x}]\text{O}_3$). PZT is piezoelectric and also ferroelectric, which means that there is a permanent net electric dipole even in the absence of any externally applied mechanical stress.

In the following, we explain the principle of the piezoelectric effect on the atomic scale using the example of a PZT unit cell. The unit cell, which is shown schematically in Fig. 3.2a, consists of Pb^{2+} at the corners of the unit cell, O^{2-} at face centered positions on the outer faces of the unit cell, forming an octahedron, and Ti^{4+} displaced from the center of the unit cell. In Fig. 3.2b, the unit cell is shown from the side with an arrow indicating the direction and size of the permanent electric dipole moment. The electric dipole inside the unit cell results in a net charge at the surfaces (xy -planes) of the piezoelectric PZT material, as in the case of a capacitor with a dielectric material inside. The direction along which the permanent dipole moment points is taken as the z -direction and the material is said to be poled along the z -direction.

When the piezoelectric material is strained in the poling direction (e.g. compressed, as shown in Fig. 3.2c), the magnitude of the electric dipole moment decreases and correspondingly the electric field inside the material and the surface charge decrease. This case, where the strain is applied along the poling direction (z -direction) leading to a voltage between the two opposite xy -surface planes, is called the longitudinal piezoelectric effect.

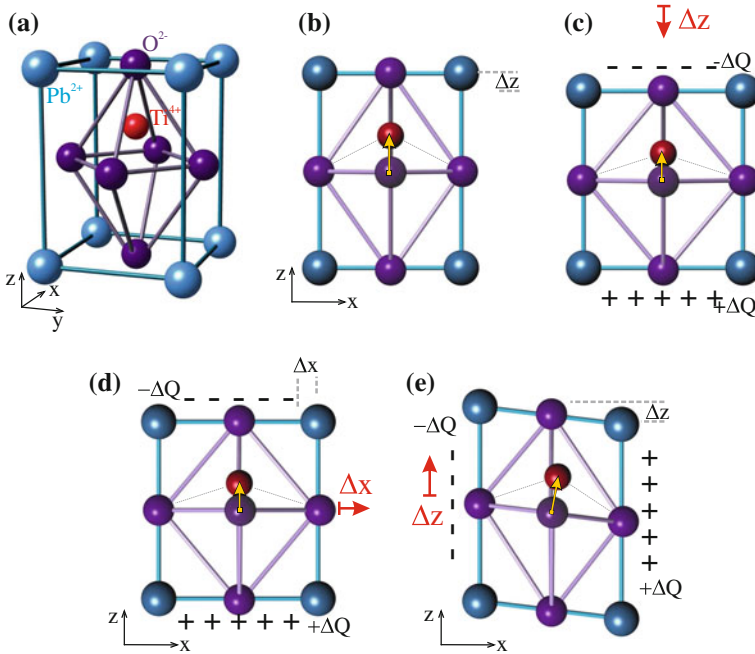


Fig. 3.2 **a** Schematic of the PZT unit cell. **b** Side view of the PZT unit cell with the dipole induced by the displaced Ti^{4+} . **c** Longitudinal piezoelectric effect: upon compression of the unit cell along the z -axis the dipole is reduced leading to a corresponding change of the surface charge. **d** Transverse piezoelectric effect: strain along the x -axis leads, due to the Poisson effect, to a change of the dipole along the z -direction and a corresponding change of the surface charge. **e** Shear piezo effect: a shear strain along the z -direction leads to a change of the x -component of the dipole and a corresponding change of the surface charge

The case in which the external strain is applied perpendicular to the poling direction (x -direction) is shown in Fig. 3.2d. In spite of the fact that the crystal is compressed in the x -direction, no dipole moment occurs in x -direction (nor in the y -direction), because there is an “inversion symmetry along the x -axis”. For every atom there is an atom at the $-x$ position inside the unit cell canceling the net dipole moment along the x -direction. However, due to the Poisson effect any strain in x -direction also leads to a corresponding transverse strain in the z -direction. This strain in the z -direction will lead to a change of the dipole moment in z -direction and to a corresponding change of the surface charge on the xy surface planes. This piezoelectric effect in which a strain along the x -direction results in a change of the dipole moment in z -direction is called the transverse piezo effect.

If a shear strain is applied along the z -direction, as shown in Fig. 3.2e, the dipole turns and induces a change of the component of the dipole moment in the x -direction and a corresponding build up of surface charge. This effect is called the shear piezoelectric effect. In the first order, the dipole moment in the z -direction does not change.

Here we discuss the piezoelectric effect. However the reverse reasoning also applies for the converse piezoelectric effect where a voltage applied to the outer

metallic electrodes results in a strain. The charge applied to the outer metallic electrodes leads to a change of the dipole moment in the piezoelectric material. This corresponds to a capacitor with a dielectric, where an charge on the capacitor plates induces a polarization and a corresponding surface charge. In the case of a piezoelectric material the dielectric is already polarized without an outer electric field applied. The change of the dipole moment (change of the polarization) induces in piezoelectric materials a corresponding strain. This direction of the piezoelectric effect is relevant for piezoelectric actuators. In the following, we describe the strain produced in different types of piezoelectric actuators induced by a voltage applied to their electrodes.

3.2 Extensions of Piezoelectric Actuators

If a voltage ΔV is applied across a rectangular piece of piezoelectric material (Fig. 3.3a) of dimensions x , y , and z (poled in z -direction) the external applied electric field is, due to the plate capacitor configuration, $\mathcal{E}_3 = \Delta V/z$. In practical terms the

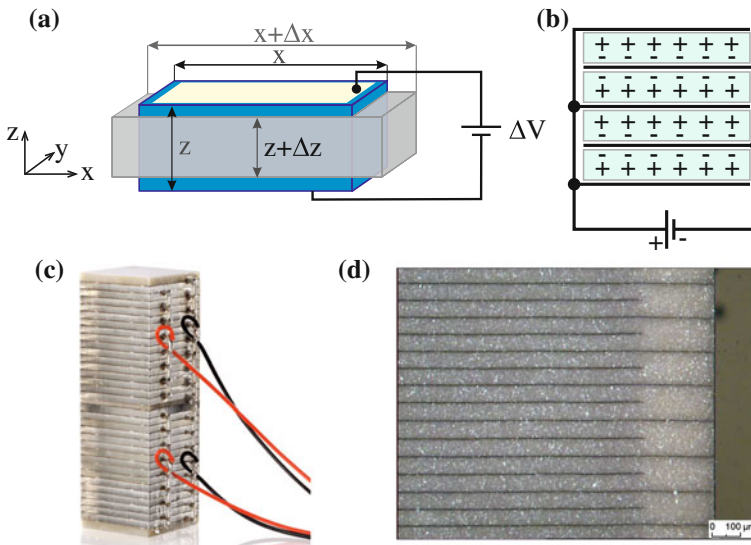


Fig. 3.3 **a** Sketch of a piezo plate (dimensions x , y , and z) poled in the z -direction. Considering the longitudinal piezo effect, an electric field in the z -direction induced by a voltage ΔV in z -direction induces a strain in z -direction, Δz . Considering the transverse piezoelectric effect a voltage in the z -direction also induces a strain in the x -direction, and also of course in y -direction. In this case, the piezo constant is proportional to the length x of the plate. **b** Since for the longitudinal piezo effect the piezo coefficient is independent of the plate thickness z , several plates have to be stacked on top of each other in order to tune (enhance) the piezo constant. **c** Photo of piezoelectric stack actuators made by gluing together single piezo plates. **d** Monolithic stack actuators with much smaller layer thickness of about $60\ \mu\text{m}$ in this case (reproduced with permission from PI Ceramic [2])

field is applied to a piece of piezoelectric material via the metallic electrodes at the surfaces of the piezo element. Often the directions x , y , and z are labeled as 1, 2, and 3, respectively. The direction of the poling field is labeled as direction 3, or as the positive z -direction. As a result of the applied electric field, a strain is generated along the z -direction and also, via the transverse contraction of the material (Poisson effect), a transverse strain in the x -direction. If a piezo plate as in Fig. 3.3a of thickness z is strained in the z -direction by Δz , the corresponding strain is $S_3 = \Delta z/z$. The strain in x -direction is $S_1 = \Delta x/x$. The same also applies for the y -direction.

The mechanical strain developed in a piezoelectric material is known to be proportional to the applied electric field, with the piezoelectric coefficients as proportionality constants. The piezoelectric coefficients are material constants which depend, however, on the direction along which the electric field is applied and on the direction along which the strain is considered. The piezoelectric coefficients are defined as the ratios of the strain components (in a certain direction) over the component of the applied electric field (in a certain direction), for example for the longitudinal piezo effect

$$d_{33} = \frac{S_3}{\mathcal{E}_3}, \quad \text{and} \quad d_{31} = \frac{S_1}{\mathcal{E}_3} \quad (3.1)$$

is the piezoelectric coefficient which applies in the case of the transverse piezoelectric effect. Because strain is a dimensionless quantity, the piezoelectric coefficients have dimensions of meter/volt. Their values are extremely small. For applications in scanning probe microscopy, a natural unit is $\text{\AA}/\text{V}$. Since the voltage difference at the electrodes and the corresponding charge difference are related to the work ΔU which has to be supplied to put charge to the electrodes by $\Delta V = \frac{\Delta U}{\Delta Q}$, equivalent units for the piezoelectric coefficients are also coulomb/newton. This is also equivalent to the induced charge density (C/m^2) per applied stress (N/m^2).

While the piezoelectric coefficients are material properties the piezo constant is assigned to a specific actuator element with specific dimensions, and the electric field applied along a specific direction, and the strain considered in a specific direction. The piezo constant is the ratio between the amount of motion in a certain direction and the voltage applied between the electrodes, e.g. $\Delta z/\Delta V$.

As a first example, a piezoelectric plate shown in Fig. 3.3 serves as our piezoelectric actuator, with the electric field applied along the z -direction (poling direction), and the strain considered in the z -direction as well. There is also strain present in the x -direction, which we will analyze later. The piezo constant $\Delta z/\Delta V$ can be calculated as follows

$$\frac{\Delta z}{\Delta V} = \frac{\Delta z/z}{\Delta V/z} = \frac{S_3}{\mathcal{E}_3} = d_{33}. \quad (3.2)$$

The piezo constant for motion of a piezo plate in the z -direction (induced by the longitudinal piezo effect) is not dependent on the thickness of the piezo plate z . The z -dependence in (3.2) is canceled out due to same dependence of both the electric field and the strain on z . This means the piezo coefficient of a plate cannot be tuned by changing its thickness (or, of course, also the diameter). The only way to tune or

enhance the length extension per voltage is to stack several piezo plates on top of each other as shown schematically in Fig. 3.3b. With common electrodes in between the plates, neighboring plates have to have opposite poling and the electrical connections to the electrodes have to be as indicated in Fig. 3.3b. A photo of this type of piezo actuator known as a piezoelectric stack actuator, produced by the company PI, is shown in Fig. 3.3c. The net displacement is the sum of the displacements of the individual piezo plates. The dimensions of the piezoelectric stack actuators are very flexible. Typical dimensions are in the mm range for the thickness of a single plate and in the cm or even decimeter range for the length of the stack. Quite large piezo constants can be achieved in this way (corresponding to a displacement of $10\ \mu\text{m}$ for a stack height of 10 mm).

There are actually two types of piezoelectric stack actuators. The first type consists of plates about half a mm in thickness, which are glued together to form a stack (Fig. 3.3c). Such stack actuators are characterized by high operating voltages of up to 1,000 V and low capacitances in the nF range. On the other hand, there are monolithic stack actuators which are characterized by a much smaller piezoelectric layer thickness ($\sim 60\ \mu\text{m}$) as shown in Fig. 3.3d. These monolithic actuators are manufactured using a cofiring technology during sintering. This type of actuator has a lower operating voltage of about 120 V. The disadvantage of such a piezo actuator is its quite high capacity, in the μF range. If a quick extension of the actuator is required, quite high charging currents have to be supplied.

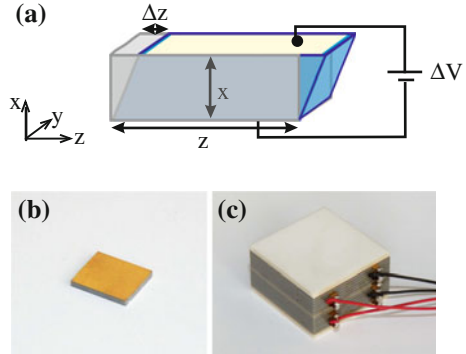
In a different kind of piezoelectric actuator, the extension of a piezo plate in x -direction due to the transverse piezoelectric effect can be exploited (Fig. 3.3a). The piezo constant for the motion along the x -axis can be obtained as

$$\frac{\Delta x}{\Delta V} = \frac{\Delta x/x}{\Delta V/z} \frac{x}{z} = \frac{S_1}{\mathcal{E}_3} \frac{x}{z} = d_{31} \frac{x}{z}. \quad (3.3)$$

In this case, the piezo constant depends on the dimensions of the plate. The piezo constant is proportional to the length x of the piezo element and inversely proportional to its thickness z . Using the transverse piezo effect, the piezo constant of the actuator can be tuned by its dimensions. To obtain a large piezo constant a long piezo or a thin piezo element can be used. However, long, thin piezo elements lead to low resonance frequencies of the bending vibration, which is disadvantageous for stable STM operation, as we will see later. For a small thickness, the electric field rises and may approach the allowed limits of the material. While we have considered a piezoelectric plate here, the most frequently used shape for a piezoelectric actuator based on the transverse piezo effect is the piezo tube, which we will consider in detail later. A piezo tube can be imagined as a plate which is rolled up to form a tube.

Of course, in a piezoelectric plate both piezoelectric effects (the longitudinal and the transverse) occur simultaneously. In both of the previous cases we focus on one effect and neglect the other due to the specific direction of the extension we are looking at. When discussing the longitudinal piezo effect of a plate we focus on the change of the thickness of the plate and neglect the change in the width of the plate

Fig. 3.4 **a** Sketch of a piezoelectric plate operated using the shear piezo effect. **b** Photo of a single shear piezo plate (6 mm × 7 mm). **c** Photo of a shear piezo stack (15 mm × 15 mm)



due to the transverse effect. On the other hand, when we focused on the transverse extension of a plate, we neglected the change of the thickness of the plate.

In Fig. 3.4a a piezoelectric plate is shown which is poled in the z -direction (horizontal in this case) while the electric field (voltage) is applied along the x -direction, i.e. vertical. As we have seen in Fig. 3.2e, this configuration leads to a shear strain along the z -direction $\Delta z/x$. In this case, the piezo constant is independent of the dimensions and is called (due to some conventions)

$$\frac{\Delta z}{\Delta V} = d_{15}. \tag{3.4}$$

As in the case of the longitudinal effect, the piezo constant does not depend on the plate dimensions. Therefore, stacks of shear piezo elements are often used here as well. Shear piezos are attractive piezo elements as they induce a uniform lateral motion of their surface. As shown in Fig. 3.4b, shear piezos have a size of only a few millimeters. If shear piezo elements are stacked onto each other and rotated by 90°, motions in two orthogonal directions can be performed as shown in Fig. 3.4c.

3.3 Piezoelectric Materials

Initially, the piezoelectric effect was observed in crystalline materials, for instance in quartz. However, for use in piezoelectric actuators, single crystals are inconvenient. Today mostly lead zirconate titanate ceramics (PZT, $\text{Pb}[\text{Zr}_x\text{Ti}_{1-x}]\text{O}_3$) are used as materials for piezoelectric actuators because ceramics can be formed into various shapes and because of their large piezo constant. These materials are ferroelectric, which means they exhibit a permanent electric dipole even in the absence of an external electric field. The unit cell of PZT has an anisotropic structure below the Curie temperature, i.e. elongated in one direction as shown in Fig. 3.5a. Above the Curie temperature, the crystal structure becomes cubic and the material loses its piezoelectric properties Fig. 3.5b.

Directly after sintering, piezoelectric ceramics does not exhibit a piezoelectric effect. This is due to two reasons: first the ceramic is a polycrystalline material with

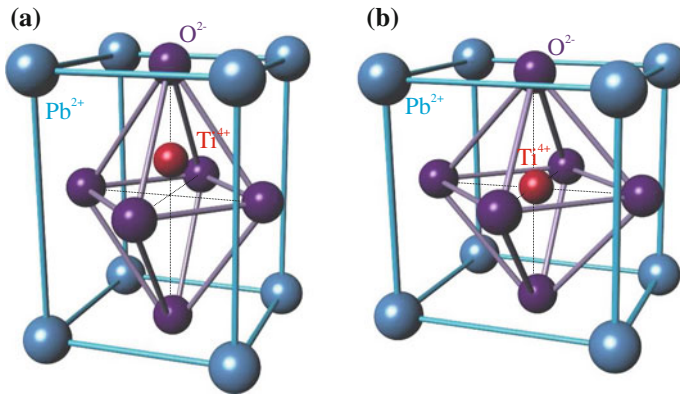


Fig. 3.5 Unit cell of the PZT crystal structure **a** below the Curie temperature **b** above the Curie temperature

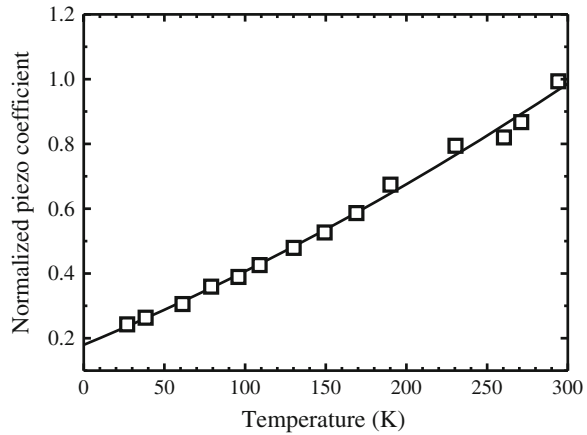
randomly oriented crystallites and second also within a single crystallite there are different domains. Inside a domain the dipoles within the unit cell are oriented in parallel, while differently oriented domains exist in one crystallite as in the case of ferromagnetism. These domains are randomly oriented in the raw piezoelectric material when it is cooled below the Curie temperature after sintering. Ferroelectric ceramics become macroscopically piezoelectric when poled. This means an electric field ($>2,000$ V/mm) is applied to the piezoelectric ceramics at temperatures somewhat below the Curie temperature. Close to the Curie temperature the crystal structure is almost cubic. With a field applied, the electric dipoles can switch (by motion of the Ti atom) to one of the six possible directions (Fig. 3.5b) which lies closest to the applied electric field. During poling, the domains can reorient and the domain walls can also move. These domains stay roughly in alignment after cooling. The material now has a remanent alignment of the dipoles, which can be degraded by exceeding the mechanical, thermal and electrical limits of the material.

Some material properties of different piezoelectric materials are listed in Table 3.1. The PZT nomenclature for the materials in Table 3.1 is an industry standard to which several companies producing piezoelectric materials refer. However, the numbers should be considered only as rough estimate since the actual values vary from man-

Table 3.1 Some properties of piezoelectric materials

Material	PZT-5A	PZT-5H	PZT-8
d_{31} ($\text{\AA}/\text{V}$)	-1.75	-2.50	-1.00
d_{33} ($\text{\AA}/\text{V}$)	3.90	6.50	3.00
d_{51} ($\text{\AA}/\text{V}$)	5.70	7.30	3.25
T_c ($^{\circ}\text{C}$)	360	220	300
Density (g/cm^3)	7.7	7.7	7.6
Young's modulus (10^{10} N/m 2)	5.7	6.3	8.9
Q	90	100	1,200

Fig. 3.6 Temperature dependence of the piezoelectric constants d_{31} for PZT-5A piezo ceramic material relative to the room temperature value (adapted from [3])



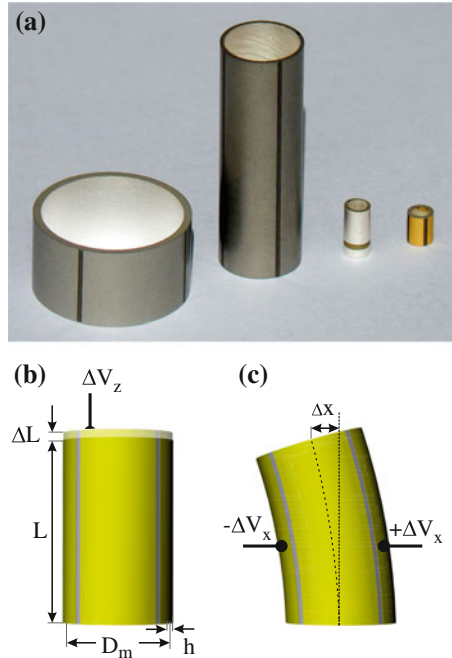
ufacturer to manufacturer. The *Curie temperature* T_c is the temperature above which the material loses its piezoelectric properties irreversibly (like a ferromagnetic material). Each material has a maximum operating temperature specified by the supplier, which is often well below the Curie temperature. The *mechanical quality factor* Q determines the sharpness of the mechanical resonance and the resonance amplitude of an actuator made from this material.

The material properties of the piezoelectric materials are also temperature-dependent. Most importantly the piezoelectric coefficients decrease for operation at low temperatures as shown in Fig. 3.6 [3] for the example of PZT-5A. As a rule of thumb, the piezo constants are for most piezo materials are roughly a factor of five lower at the temperature of liquid helium than at room temperature.

3.4 Tube Piezo Element

One central task in scanning probe microscopy is to position the probe with an accuracy of less than one tenth of an ångström in all three dimensions. The tube piezo element (or tube scanner) is the most widely used actuator element to move the probe tip or the sample in order to scan a surface (fine motion). One single tube piezo element allows motions to be performed in three orthogonal directions. Further advantages are high piezo constants and high resonance frequencies. The tube scanner consists of a tube, made of piezoceramics (poled in radial direction), which is covered inside and outside with metal electrodes. The outer electrode is divided into four quadrants, as shown in Fig. 3.7. A motion in the z -direction (along the longitudinal axis) can be achieved by applying a voltage between the inner and all outer electrodes (Fig. 3.7b). A deflection in the xy -direction is induced by voltages of opposite polarity applied to the two opposite outer electrodes Fig. 3.7c. Due to the transverse piezoelectric effect, one segment of the tube extends along the tube axis,

Fig. 3.7 **a** Photograph of several tube piezo elements. **b** Schematic *side view* of a tube scanner showing the vertical extension along *z*. **c** Schematic of the lateral movement in the *x*-direction



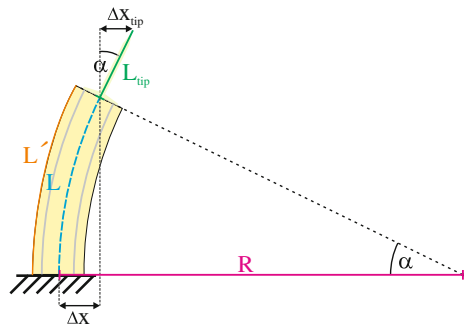
while the opposite segment shrinks, giving rise to a bending of the upper part of the tube, as shown in Fig. 3.7c. When a tube scanner is used to scan a tip, the tip (holder) is mounted axially on top of the tube scanner.

The vertical displacement $\Delta L = \Delta z$ of the top of the tube scanner is calculated using (3.3) (exchanging the directions *x* and *z*), leading to the following piezo constant

$$\frac{\Delta z}{\Delta V} = d_{31} \frac{L}{h} \tag{3.5}$$

In order to obtain the lateral displacement Δx of the tube, we assume that the bending of the tube follows a circular arc as shown in Fig. 3.8. From this figure, we identify

Fig. 3.8 Sketch of the geometry of a bent piezo tube with the relevant parameters



(due to the definition of the arc length) the bending angle as

$$\alpha = \frac{L}{R}. \quad (3.6)$$

Further, we identify $L' = L + \Delta L$, which can also be written as

$$L' = \alpha \left(R + \frac{D_m}{2} \right) = L + \alpha \frac{D_m}{2}. \quad (3.7)$$

This results in

$$\alpha = 2 \frac{\Delta L}{D_m}, \quad (3.8)$$

with D_m being the mean diameter of the tube. From Fig. 3.8 we also determine that the cosine of the bending angle can be written as

$$\frac{R - \Delta x}{R} = \cos \alpha \approx 1 - \frac{\alpha^2}{2}. \quad (3.9)$$

Thus the x -deflection of the tube is given by

$$\Delta x = \frac{R\alpha^2}{2}. \quad (3.10)$$

Replacing R using (3.6) and (3.8) results in the following expression for the x -deflection of the tube

$$\Delta x = \frac{\Delta L L}{D_m}. \quad (3.11)$$

For the length extension ΔL of the piezo tube we can make the simplified assumption that it is the vertical length extension according to (3.5). With this assumption the piezo constant for the x -deflection results as

$$\frac{\Delta x}{\Delta V} = \frac{d_{31} L^2}{D_m h}. \quad (3.12)$$

A better approximation for the length extension ΔL , which considers non uniform stress in the electrodes due to bending, is considered in Appendix A and results in the following expression for the piezo constant for horizontal bending

$$\frac{\Delta x}{\Delta V} = \frac{2\sqrt{2}}{\pi} \frac{d_{31} L^2}{D_m h}. \quad (3.13)$$

This equation corresponds to the bipolar operation of the tube where voltages $-\Delta V$ and $+\Delta V$ are applied to opposite electrodes.

Typical dimensions of a piezo tube (PZT-5A) are as follows: length 25.4 mm, mean diameter 5.84 mm, wall thickness 0.51 mm, which results in a piezo coefficient for x and y directions of $725 \text{ \AA}/V$ and for the z -direction of $90 \text{ \AA}/V$. The most effective design parameter to tune the piezo coefficient is the length of the tube, as the xy -piezo coefficient is quadratically dependent on the tube length.

What we have considered up to now is the deflection of the top of the piezo tube. However, if a tip is mounted on a scanner tube, it is usually mounted at a distance L_{tip} above the center of the piezo tube. In this case, an additional deflection Δx_{tip} results, which can be written according to Fig. 3.8 and using (3.6) and (3.8) as

$$\Delta x_{\text{tip}} = L_{\text{tip}} \sin \alpha \approx L_{\text{tip}} \alpha = L_{\text{tip}} \frac{2\Delta L}{D_m} = L_{\text{tip}} \frac{4\sqrt{2}}{\pi} \frac{d_{31} L \Delta V}{D_m h}. \quad (3.14)$$

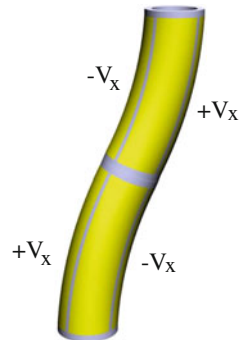
Combining this with (3.13), the total piezo constant for the horizontal deflection results in

$$\frac{\Delta x_{\text{tot}}}{\Delta V} = \frac{\Delta x + \Delta x_{\text{tip}}}{\Delta V} = \frac{2\sqrt{2}}{\pi} \frac{d_{31} L_{\text{piezo}}}{D_m h} (L_{\text{piezo}} + 2L_{\text{tip}}), \quad (3.15)$$

denoting the length of the piezo tube as L_{piezo} .

One disadvantage of the tube scanner is the fact that x , y and z motions are not completely decoupled. The x , y motion acts approximately on a sphere. Therefore, every lateral motion also results in a slight motion in the z -direction and vice versa. This is because the tube scanner relies on bending and not on linear motion. There is a method to prevent this coupling [4]. As shown in Fig. 3.9, a z displacement can be prevented during an xy -motion by an opposite bending in the upper part of the piezo which now has eight electrodes on the outer side. With this trick, good linearity in x and y directions is achieved and a coupling with the z -displacement is eliminated. The disadvantage of this type of scanner is that the scan range in x and y direction is reduced by a factor of two for a given piezo length.

Fig. 3.9 Instead of an outside electrode divided into four segments the outer electrode has eight segments. The *upper part* of the piezo is bent in the opposite direction to prevent a displacement in the z -direction



3.4.1 Resonance Frequencies of Piezo Tubes

Here we summarize equations for the resonance frequencies of tubes, and also of beams such as those used as cantilevers in atomic force microscopy, taken from [1]. These equations are obtained using the assumptions underlying the (classical) Euler-Bernoulli beam theory, which are the proportionality of stress and strain (small bending), as well as the condition that a plane cross section of the beam remains plane under bending, i.e. shear deformations are ignored. As a boundary condition it is assumed that one end of the tube (beam) is rigidly fixed to a rigid wall.

The frequency of the lowest longitudinal (axial) vibrational stretching mode of a rod or tube with one end clamped and one end free is

$$f_{\text{stretch}} = \frac{\lambda_i}{2\pi L} \sqrt{\frac{E}{\rho}}, \quad (3.16)$$

where L is the length of the beam, ρ is its volume density, and E Young's modulus.¹ The value of λ_i for the i th resonance is given by $\lambda_i = \pi/2 \cdot (2i - 1)$. For the lowest resonance ($i = 1$) the stretching frequency results as

$$f_{\text{stretch}} = \frac{1}{4L} \sqrt{\frac{E}{\rho}} = \frac{c}{4L}, \quad (3.17)$$

where c is the longitudinal velocity of sound, which is given in long rods as $c = \sqrt{E/\rho}$. For a mass M at the end of the beam (tube) the following expression holds for the lowest axial resonance frequency

$$f_{\text{stretch}} \approx \frac{1}{2\pi} \sqrt{\frac{AE}{ML}}, \quad (3.18)$$

with A being the cross sectional (material-containing) area of the beam (tube).

The resonance frequencies of the bending modes of a beam (perpendicular to the beam axis) clamped at one end and free at the other end are given by

$$f_{\text{bend}} = \frac{\lambda_i^2}{2\pi L^2} \sqrt{\frac{EI}{\rho A}} = \frac{\lambda_i^2 \kappa}{2\pi L^2} \sqrt{\frac{E}{\rho}}. \quad (3.19)$$

The values for λ_i are 1.875 and 4.694 for the first two modes, respectively. The dimensions of the beam enter into the area moment of inertia (also called second moment of inertia) $I = \int z^2 dA$, where z is the direction of bending. The expression $\sqrt{I/A} = \kappa$ is called the radius of gyration and has the following expressions: for a

¹ In tables sometimes also the elastic compliance S is used, which corresponds to the reciprocal of Young's modulus.

circular rod $\kappa = D/4$, for a tube $\kappa = \sqrt{D^2 + d^2}/4$, with D being the outer diameter and d inner diameter. For a tube with negligible wall thickness $\kappa = D/(2\sqrt{2})$ results, and for a beam with rectangular cross section (with width w and thickness t) $\kappa = \frac{1}{12}wt^3$ results for bending in the direction of the thickness.

With an additional mass M at the end of the beam and the mass of the beam m , the first resonance frequency can be expressed as

$$f_{\text{bend}} = \frac{1}{2\pi} \sqrt{\frac{3EI}{L^3(M + 0,2357m)}}. \quad (3.20)$$

Simple numeric estimates for the resonance frequencies are obtained from these equations. As an example, we consider the lowest bending frequency of a tube. Following (3.19) the bending frequency results as

$$f_{\text{bend}}^{\text{tube}} = \frac{0,56\sqrt{D^2 + d^2}}{4L^2} \sqrt{\frac{E}{\rho}}. \quad (3.21)$$

For a PZT-5A tube with the dimensions length 12 mm, outer diameter 3.2 mm, and inner diameter 2.2 mm, the calculated resonance frequencies are 56 and 10.1 kHz for the stretching and the bending mode, respectively. These resonance frequencies can also be measured experimentally in a setup like the one shown in Fig. 3.10a. An AC voltage is applied to one of the four outer electrodes. Due to the piezoelectric effect the tube bends and a voltage is induced by the piezoelectric effect on the opposite electrode (the two other outer electrodes and the center electrode are grounded, as shown in Fig. 3.10a). This kind of excitation excites the bending modes. The first bending resonance is measured at 9.3 kHz (Fig. 3.10b), which corresponds roughly to the calculated value of 10.1 kHz. The higher frequencies around 42 kHz correspond to the second bending mode and do not correspond so well to the calculated value of 62 kHz. Figure 3.10c shows the configuration for the excitation of the stretching mode. The measured frequency of 49 kHz corresponds roughly to the calculated frequency of 56 kHz.

Generally, the bending resonance frequencies are overestimated by the equations for two reasons: the neglect of shear forces in the Euler-Bernoulli theory and the idealized boundary conditions. At one end, the tube (beam) is considered to be fixed rigidly to a stiff support. However, the support has some elasticity and, if the tube is glued to the support, also its elasticity enters into the considerations.

If tube piezos have been depolarized, e.g. by too high temperature, they can be repolarized by applying a DC voltage between the inner and outer electrodes (the polarity should be the same as during poling, which is different for different manufacturers). The necessary voltage depends on the wall thickness of the tube. An electric field of about twice the coercitive field (cf. Fig. 3.12) should be used for several hours at room temperature, or rather at elevated temperature but still below the Curie temperature.

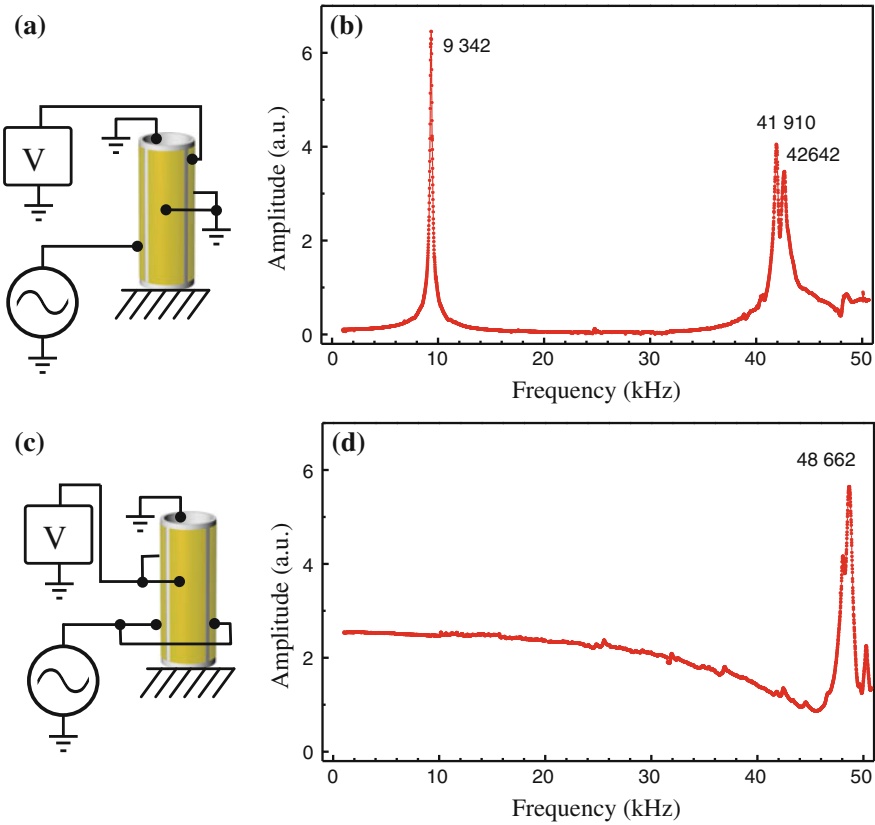


Fig. 3.10 **a** Schematic of the measurement setup with an electric excitation of the mechanic oscillation of a tube piezo element (bending mode). The amplitude of the mechanically excited oscillation is detected by the piezoelectric effect. **b** Amplitude of the mechanic oscillation. Resonances are observed at the first bending mode at 9.3 kHz and at the second bending mode around 42 kHz. **c** Schematic setup for the excitation of the stretching mode. **d** The first stretching resonance frequency is measured at 49 kHz

3.5 Flexure-Guided Piezo Nanopositioning Stages

A further continuously moving nanopositioning system uses flexure guides. It relies on the elastic deformation of a spring-like structure which confines the motion in only one direction and is driven by a piezo element. The working principle can be seen in Fig. 3.11a. In a metal block, small trenches are cut by wire EDM (Electrical Discharge Machining). These trenches are shaped in a meandering way so that they allow a spring-like motion along one direction for the material inside, while being stiff along the other directions. A second set of trenches forms flexures to guide the motion along the orthogonal direction. Stacks of piezo elements (blue in Fig. 3.11a) are used to move the flexures. Sometimes a mechanical lever is included

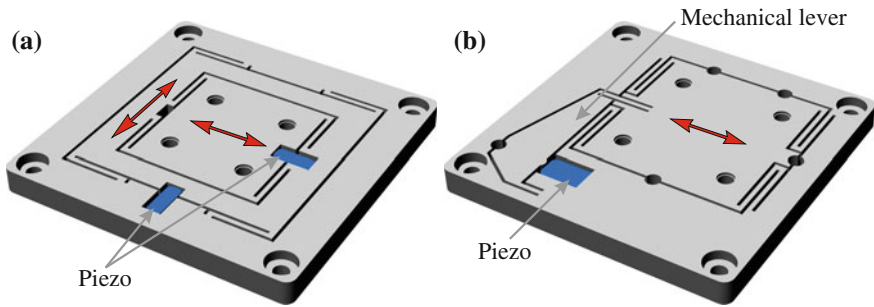


Fig. 3.11 **a** Flexure-guided piezo nanopositioning xy -stage. **b** Flexure-guided piezo stage with an integrated mechanical lever amplifying the motion

in the flexures (Fig. 3.11b) in order to amplify the motion ranges up to hundreds of micrometers. Capacitive position sensing detectors can be integrated to allow a precise measurement of the motion. One disadvantage of the flexure-guided piezo nanopositioning stages is that they are relatively large.

3.6 Non-linearities and Hysteresis Effects of Piezoelectric Actuators

The positioning performance of piezoelectric actuators is limited by the effects of hysteresis and non-linearities, which will be discussed in the following.

3.6.1 Hysteresis

There are mainly two contributions which lead to a strain of a piezoelectric ceramic in the presence of an outer electric field. The intrinsic effect results from the displacement of the ions inside the crystal lattice in the presence of an electric field, as shown in Fig. 3.5a. This effect is approximately linear and non-hysteretic.

A second extrinsic contribution results from the reorientation of the ferroelectric domains present in the crystal lattice. A ferroelectric ceramic consists of sintered crystallites which have a random orientation of their crystalline lattice. Inside a crystallite, ferroelectric domains with different orientations exist as follows. As seen in Fig. 3.5, the Ti ion in the crystal lattice can move in six different directions, and domains with six different orientations (ferroelectric domains) can exist in the crystal lattice. The ferroelectric domains with their inner electric field parallel to the outer applied field have lowest energy and the domains with anti-parallel orientation have the highest energy. Thus there is an energetic tendency for a reorientation of the domains parallel to the applied electric field. However, there is also an intrinsic

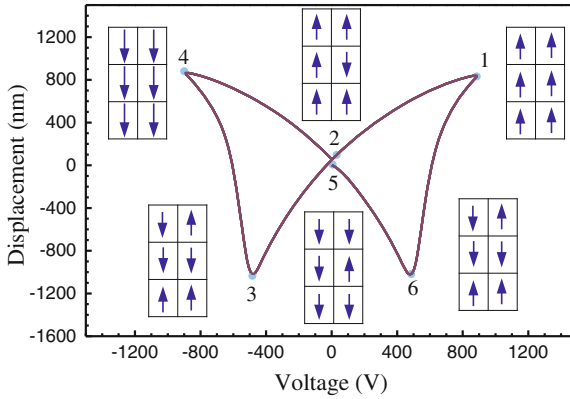


Fig. 3.12 The *butterfly curve* of the piezoelectric material PIC 151 [2] for the applied field and the displacement, both in 3-direction. The strain is shown in dependence of the applied electric field for large electric fields. The corresponding polarization of ferroelectric domains is also indicated in a simplified scheme. The *butterfly curve* shown here was kindly measured by aixACCT [5]

energetic barrier which has to be overcome by the Ti atom when jumping from one of the six directions to another one.² With increasing and decreasing electric field the sizes of different domains change. Due to the barriers which have to be overcome to reach a low energy state, the inner state of the system (roughly the volume of each domain orientation) depends on the history of the system leading to the hysteretic behavior.

Hysteretic behavior in general means that the response of the system (extension of the piezo) does not only depend on the external conditions (applied electric field in our case), but also on the internal state of the system (i.e. its history and here specifically the state of the domain structure). The hysteresis behavior of a piezoelectric ceramic is usually shown in a butterfly curve, where the strain is plotted in dependence of the applied electric field (Fig. 3.12). This figure also shows a schematic sketch of the polarization in the domains. The domains are considered to be square and aligned with respect to the applied field. Also only two of the six possible domain orientations are considered. Point 1 corresponds to saturation polarization where all domains are aligned and also corresponds to maximum strain. If the electric field is subsequently reduced to zero the point of remanent polarization is reached (point 2), where most of the dipoles are still oriented parallel to the outer field. This state corresponds to a certain remanent strain. Between point 1 and point 2 the strain is mainly induced by the intrinsic piezoelectric effect. When the electric field changes orientation the domains also begin to reverse their orientation and the strain is increasingly also induced by domain reorientation. Approaching point 3, the net

² In this simplified consideration, we have left out the formation energy of domain walls which results in the formation of larger domains. Larger domains mean less domain wall energy. A further contribution in the energy balance is the build up of mechanical strain inside the domains when an external electric field is applied.

polarization of the domains is zero. With an increased electric field in the opposite direction the domains begin to align to the opposite direction and correspondingly the strain increases again to its maximum value (point 4). When the electric field is subsequently reversed again, the strain follows a different curve from point 4 to point 5 to point 6 and to point 1. This means that the strain induced by domain reorientation is subject to hysteresis, i.e. depends not only on the external applied electric field but also on the history or the internal state of the system.

The butterfly curve shows the large signal response of piezoelectric ceramics. The working range of piezoelectric materials is between point 1 and point 2 for unipolar operation. For bipolar operation which is used to drive tube piezo elements in scanning probe microscopy, point 3 must not be reached because it corresponds to a depolarization of the piezo. Usually only electric fields substantially below the point of depolarization should be used.

In Fig. 3.13, smaller voltage signals which are used for scanning in SPM are shown together with the corresponding displacement. Also here a hysteresis is visible indicated by the elliptic curves which correspond to voltage sweeps from zero to a maximal voltage and back to zero (indicated by the arrows). Such a voltage sweep corresponds to scanning one line in an SPM image. Two effects are observed during these voltage sweeps: first the displacement is different for increasing and decreasing voltages and second this hysteresis increases for larger voltage amplitudes.

Due to this hysteretic behavior the piezo constant (displacement divided by voltage) is not constant anymore. The piezo “constant” depends on the applied voltage and also on the history of the system (which voltages were applied before). If we define the maximum displacement divided by the maximum voltage during one voltage sweep as average piezo constant for this voltage sweep, we see that this average

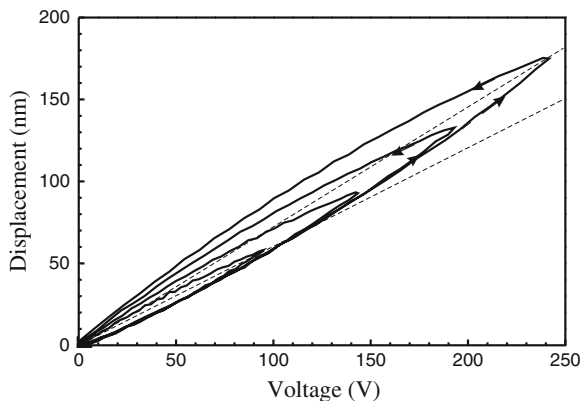


Fig. 3.13 The displacement induced by an applied voltage also shows hysteretic behavior in a range up to 200 V for the applied voltage and the displacement, both in 3-direction. The average piezo constant indicated by the *dashed lines* increases for increasing voltage amplitudes. Due to this the piezo constants and the corresponding displacements can vary by 10–25 %. The curves shown here was kindly measured by aixACCT [5] on a PIC 151 ceramic [2]

piezo constant increases with the voltage amplitude. This effect results from the increasing contributions due to extrinsic domain reorientation at larger voltages. The average piezo constants are indicated by dashed lines in Fig. 3.13 for the two voltage sweeps with smallest and largest amplitudes. The average piezo constant for the smallest and the largest voltage sweeps in Fig. 3.13 differ by about 18 % in this case. This means that due to the effect of hysteresis the piezo constant and correspondingly the piezo displacements vary by 10–25 % for different voltages.

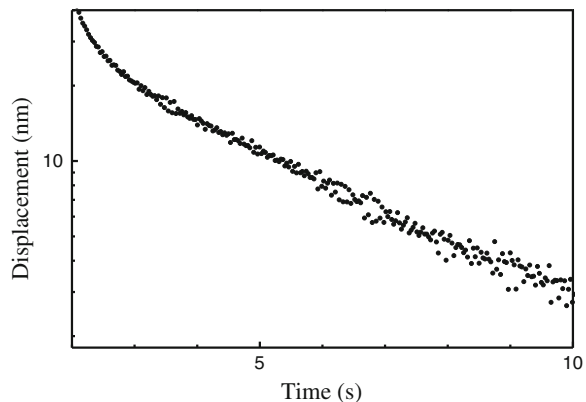
This variation (increase) of the piezo constant for larger voltages leads to significant image distortions at larger scan sizes, visible for instance when imaging defined gratings on the scale of several micrometers. The piezoelectric coefficients quoted by the manufacturers of piezo elements are those in the small voltage limit.

3.6.2 Creep

When considering hysteresis (i.e. the domain orientation in dependence of the applied electric field), always a very slow, quasi-static change of the electric field was considered. Since the domain reorientation is an energetically activated process, this process also depends on time. In the case of an instantaneous change of the electric field, the domain reorientation (domain wall motion) and the subsequent build-up of strain (extension of the piezo) do not happen instantaneously but take some time after the electric field has been established. As a result of a sudden jump in the voltage applied to the piezo electrodes the change in position is not instantaneous. A certain time dependence of the position, called creep, is observed. A measurement of creep (displacement as function of time) for short times after an instantaneous voltage jump is shown in Fig. 3.14. For an ideal piezo actuator without creep the displacement would occur only at the time of the voltage jump and not change afterward.

In SPM, the creep results in an effect at the turning points of the scanning movements of each scan line. A positive piezo extension still occurs due to creep, while

Fig. 3.14 Creep is the piezo displacement after an instantaneous voltage jump. The curve shown here was kindly measured by aixACCT [5] on a PIC 151 ceramic [2]



the voltage change has already reversed its direction. In the vertical direction creep occurs after the (rapid) approach of the tip to the sample. During the approach process, large variations of the z -position are usual and after the approach to the surface a creep in z results.

Creep and hysteresis are also the reason why in scanning probe methods two successive scan lines should not be scanned in opposite directions (first line: $+x$, second line $-x$, ...) but always in the same direction (first line: $+x$, second line $+x$, ...) (no data are acquired while scanning backwards in the $-x$ -direction). For lines scanned in opposite directions, a mutual shift in the position of up to 20% would result due to creep and hysteresis.

3.6.3 Thermal Drift

Thermal drift of the mechanical setup leads to image distortions. This is a general effect on all mechanical components of the microscope, and is not limited to piezo elements; specifically, when the sample has been previously annealed (for instance in the process of sample cleaning). Usually it takes some time after approach before the thermal drift is reduced sufficiently for imaging. In low temperature experiments thermal drift is suppressed.

In conclusion, due to all the above mentioned limitations for piezoelectric scanners, scanning probe techniques are generally not suitable tools for a *quantitative* measurement of distances in the micrometer range (without careful separate calibration). If atomic resolution is achieved the lateral calibration can be performed by taking atomically resolved images of a known surface structure. The vertical calibration is usually performed at (single) monoatomic step edges. If no atomic resolution is obtained, commercially available calibration grids can be used for horizontal and vertical calibration.

An absolute calibration of scanners is also possible using interferometric or capacitive position sensors. In this case, a closed loop operation can be realized. In a feedback loop, the voltage at the piezoelectric actuator is adjusted such that the desired and measured displacement of the actuator is reached. This is the best way to eliminate all effects of piezo hysteresis and creep. However, the measurement of the piezo extension results in larger sizes of the piezoelectric actuator. Also an increased number of cables and additional control electronics are needed. Nowadays, closed loop operation is standard in atomic force microscopes.

3.7 STM Tip Preparation

Tip preparation is an important point, which defines the resolution of the scanning tunneling microscope and the quality of the images. The tip should have a minimal radius of curvature at the end and a narrow diameter to penetrate into trenches and pits on the surface. The tip material should be stable in high electric fields.

Tips for STM under ambient conditions are typically made of platinum or a Pt-Ir wire in order to prevent oxidation of the tip material in air. A more or less sharp tip can be produced by cutting and/or grinding. These crude tip preparation techniques are only used for scanning very flat surfaces like graphite. For STM in vacuum, electrochemically etched tungsten tips are most frequently used. The most common procedure of electrochemical etching is the DC drop-off method [6]. A tungsten wire (diameter 0.25 mm) is put into a solution of NaOH (e.g. 5 g NaOH in 50 ml water) and kept at a positive potential towards a stainless steel counter electrode (Fig. 3.15a). The etching process takes place predominately near the surface of the solution. Due to convection, fresh OH^- is supplied from the air-electrolyte interface. The downward flow of the heavy W anions protects the lower part of the wire in the electrolyte from the supply of fresh OH^- . These specific conditions lead automatically to the formation of a narrow neck shown in Fig. 3.15a. When the neck is etched thin enough the wire fractures due to its weight. Additionally, in order to prevent any further etching, the etching voltage is shut down by the control electronics. The remaining top part will be used as the tip (Fig. 3.15b) and has to be cleaned with deionized water. Most often the tip is covered with an oxide layer and contaminations from the etchant. Thus other in vacuum treatments of the tip, like annealing or field evaporation, are often applied.

There are several different types in situ (in vacuum) tip treatment. Due to the fact that the real sharpness of the tip on the atomic scale cannot be accessed these treatments often have the character of highly empirical procedures. In the following, some examples of further cleaning and characterization in vacuum are given.

Heating. The freshly etched tip is fixed in a special tip-holder and installed into a load-lock chamber for transfer to vacuum. Resistive heating of the tip apex can be performed in order to remove the oxide layer and other contaminations remaining

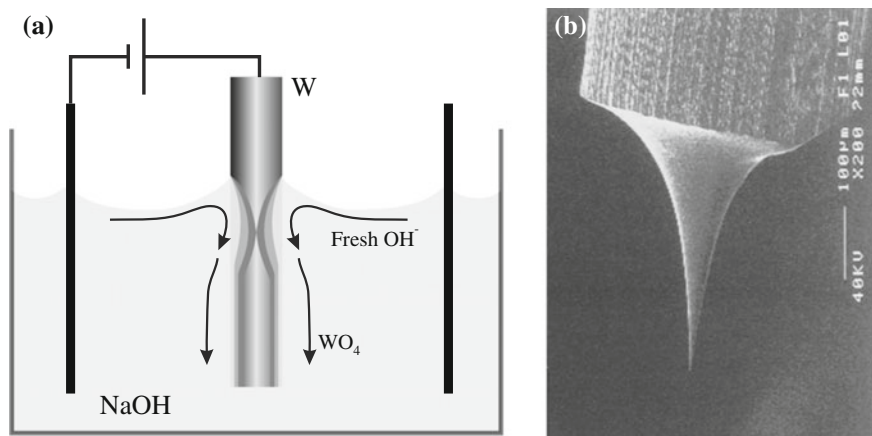


Fig. 3.15 **a** Schematic of electrochemical tip etching. **b** SEM image of an etched tip, original wire diameter 0.25 mm

after the chemical etching [7]. A direct current is applied between the tip and a tungsten wire (diameter 0.5 mm) that touches the tip wire at a point near to the tip apex. The tip should be heated to a temperature above 800°C for several seconds. The sharpness of the tip is controlled by the value of the applied voltage required in order to achieve a certain field emission current from the apex of the tip. It was found that to obtain an emission current of 1 nA, the applied voltage should not exceed 600 V. If a higher voltage than 600 V is required the tip has a poor sharpness and has to be changed. The pressure during this operation should be less than about 10^{-8} mbar. After this second step of tip preparation, the tip is introduced into the tunneling microscope by the transfer system. Another way of heating the tip is heating by electron bombardment.

Sputtering. Ion bombardment of the tip under vacuum conditions (for instance Ar ions at several hundred volts) can be used to clean and sharpen the tip.

High field treatment. It is also possible to sharpen the tip during tunneling. The bias voltage is raised for a short time (for several scan lines) to several volt (negative at the sample). By this treatment some W atoms may diffuse to the tip apex due to the non-uniform electric field and form a nanotip.

Tip indentation into metal. It is also possible to reshape a blunt tip by indenting (pressing) it several nm into a soft metal sample. In this way a new microtip can be formed. This is also the reason why, when working on metal samples, the tip is rarely replaced.

3.8 Vibration Isolation

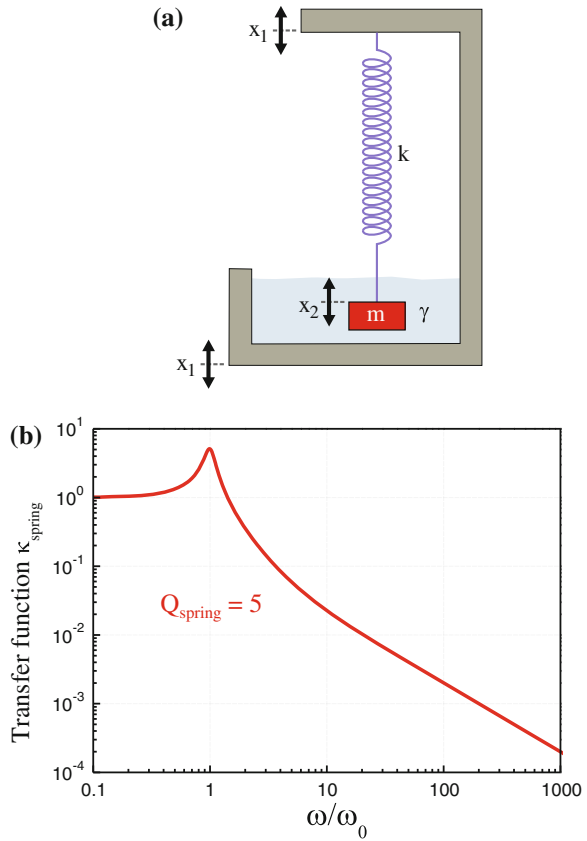
In order to keep the scanning probe stable with respect to the sample with an accuracy of less than 0.1 \AA would (ambitiously) require a vibrational noise level of about a factor of ten lower than this for the relative motion between tip and sample, i.e. 1 pm. In this case, the usual amplitudes of building vibrations of $\sim 0.1 \mu\text{m}$ have to be reduced by a factor of 100,000 for the tip-sample distance. As we will see in the following, to accomplish this task both good vibration isolation and a rigid microscope have to be combined.

We will perform the analysis of the vibration isolation in two steps. In the first step, we will consider the microscope as a rigid construction of mass m and ask: How can this mass be isolated from outside vibrations? In the second step, we also consider the microscope itself as a oscillating system where the tip oscillates against the sample and we ask: How can these tip-sample oscillations be reduced?

3.8.1 Isolation of the Microscope from Outer Vibrations

If the microscope is considered as a rigid mass, outside vibrations are transmitted from the ground and the air. An effective vibration isolation can be obtained by

Fig. 3.16 a Vibration isolation of a microscope (represented by a mass m) against external vibrations x_1 using a spring suspension. **b** Transfer function of the vibration isolation system for $Q_{\text{spring}} = \omega_0/\gamma = 5$



a spring suspension (Fig. 3.16a). The microscope assembly (mass m) is fixed to a spring with spring constant k . This harmonic oscillator has a natural frequency of $\omega_0 = \sqrt{k/m}$. The oscillating system is damped with a damping factor γ (or the corresponding quality factor $Q_{\text{spring}} = \omega_0/\gamma$). An external (sinusoidal) vibration $x_1(t)$ with amplitude x_1^0 and frequency ω (vibration from of the building floor) is coupled into the system (Fig. 3.16a). As a reaction to this outside forced excitation, the mass m performs an oscillation $x_2(t)$ with amplitude x_2^0 at the driving frequency ω . We refer the motions x_1 and x_2 relative to a fixed (not oscillating) reference system. The elastic force on the mass depends on the *difference* of the positions ($x_2 - x_1$). Thus the restoring force of the spring acting on the mass m is

$$F_{\text{spring}} = -k(x_2 - x_1), \tag{3.22}$$

In the current case, it is assumed that the frictional damping force depends on the *difference* of the velocities³ $(\dot{x}_2 - \dot{x}_1)$. Therefore, the damping force F_{frict} is

$$F_{\text{frict}} = \gamma m(\dot{x}_2 - \dot{x}_1). \quad (3.23)$$

The equation of motion for the mass m reads now

$$\ddot{x}_2 + \gamma(\dot{x}_2 - \dot{x}_1) + \omega_0^2(x_2 - x_1) = 0, \quad (3.24)$$

or reordered slightly

$$\ddot{x}_2 + \gamma\dot{x}_2 + \omega_0^2x_2 = \gamma\dot{x}_1 + \omega_0^2x_1. \quad (3.25)$$

For a sinusoidal vibration of the frame x_1 can be written in the complex notation (skipping the tilde)

$$x_1(t) = x_1^0 e^{i\omega t}, \quad (3.26)$$

the steady-state solution for the motion of the mass m is

$$x_2(t) = x_2^0 e^{i\omega t}. \quad (3.27)$$

with x_1^0 and x_2^0 being complex amplitudes which include a relative phase shift between the two amplitudes.

Substituting (3.26) and (3.27) into (3.25) we obtain (again using the power of the complex method: differentiation is just multiplication by $i\omega$)

$$-\omega^2 x_2 + i\gamma\omega x_2 + \omega_0^2 x_2 = i\gamma\omega x_1 + \omega_0^2 x_1. \quad (3.28)$$

or

$$(-\omega^2 + i\gamma\omega + \omega_0^2)x_2^0 e^{i\omega t} = (i\gamma\omega + \omega_0^2)x_1^0 e^{i\omega t}. \quad (3.29)$$

Finally, we obtain

$$\frac{x_2^0}{x_1^0} = \frac{\omega_0^2 + i\gamma\omega}{\omega_0^2 - \omega^2 + i\gamma\omega}. \quad (3.30)$$

This ratio is still a complex number, since both amplitudes are complex quantities having a real amplitude and phase. The ratio of the absolute values of the amplitudes is called the transfer function of the vibration isolation system $\kappa_{\text{spring}}(\omega)$, which can be written as

$$\kappa_{\text{spring}}(\omega) = \frac{|x_2^0|}{|x_1^0|} = \sqrt{\frac{\omega_0^4 + \gamma^2\omega^2}{(\omega_0^2 - \omega^2)^2 + \gamma^2\omega^2}}. \quad (3.31)$$

³ If the damping medium is at rest relative to a fixed external coordinate system, (i.e. not oscillating together with x_1 , as assumed here), the term \dot{x}_1 has to be neglected in the following. This case applies to a cantilever in atomic force microscopy damped in air.

The response of the system to a driven oscillation $\kappa_{\text{spring}}(\omega)$ can be divided into three regimes (Fig. 3.16b). For $\omega \ll \omega_0$ the outside excitation is transmitted with a transfer function of one, i.e. without any damping. For a frequency close to the natural frequency of the system (in resonance), the outside excitation is even amplified, i.e. the vibrations are increased instead of damped. At $\omega = \omega_0$ the transfer function at becomes

$$\kappa_{\text{spring}}(\omega_0) = \sqrt{\frac{\omega_0^4 + \gamma^2 \omega_0^2}{\gamma^2 \omega_0^2}} = \sqrt{1 + \frac{\omega_0^2}{\gamma^2}} = \sqrt{1 + Q_{\text{spring}}^2}. \tag{3.32}$$

For small damping ($\gamma \ll \omega_0$ or equivalently $Q_{\text{spring}} \gg 1$), the transfer function can be approximated by

$$\kappa_{\text{spring}}(\omega_0) \approx \frac{\omega_0}{\gamma} = Q_{\text{spring}}. \tag{3.33}$$

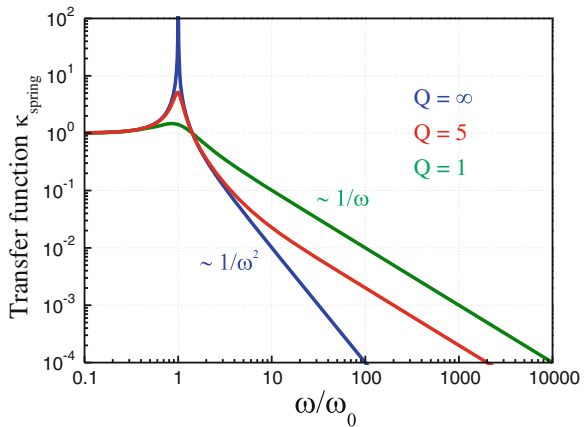
If the Q -factor is very large, the external vibration would be amplified tremendously at ω_0 . To avoid such resonance excitation, appropriate damping must be applied.

In the third regime $\omega \gg \omega_0$ and γ approaching zero (or correspondingly Q_{spring} very large), the transfer function (3.31) reduces to

$$\kappa_{\text{spring}}(\omega) \approx \left(\frac{\omega_0}{\omega}\right)^2. \tag{3.34}$$

This shows that for excitation frequencies ω much larger than the natural frequency ω_0 and for small damping, the external vibrations are suppressed $\sim 1/\omega^2$. We have seen that damping (small Q -factor or large γ) avoids resonance excitation. However, on the other hand damping deteriorates vibration isolation at higher frequencies. The transfer function becomes asymptotically $\sim 1/\omega$ for $Q_{\text{spring}} = 1$. In Fig. 3.17 the transfer function is shown for different values of Q_{spring} . In typical spring suspen-

Fig. 3.17 Transfer function of a spring suspension system for different values of the quality factor Q_{spring}



sion systems, a compromise between good damping at high frequencies and large resonance enhancement is chosen for $Q_{\text{spring}} \approx 2 - 5$.

The best vibration isolation (for instance from building vibrations) is achieved with the lowest natural frequency of the spring system. Therefore, the natural frequency of the spring system is the prime parameter of a vibration isolation system. In the following, we will show that this parameter only depends on the extension length of the spring Δl .

Hooke's law results in $k\Delta l = mg$. If we insert the result for m into the equation for the natural frequency of the system $f_0 = \frac{1}{2\pi}\sqrt{k/m}$ the natural frequency for the system can be written as

$$f_0 = \frac{1}{2\pi}\sqrt{\frac{k}{\Delta l k/g}} = \frac{1}{2\pi}\sqrt{\frac{g}{\Delta l}}. \quad (3.35)$$

To achieve a natural frequency of 1 Hz the spring should be stretched by 25 cm. To achieve a natural frequency of 0.5 Hz the spring has to be stretched by 1 m. This length is difficult to integrate in a system. Some reduction of the length of the springs can be achieved by using pretensioned springs. Such springs are available in principle, but, it is difficult to manufacture springs which simultaneously feature a high pretension force and a low natural frequency.

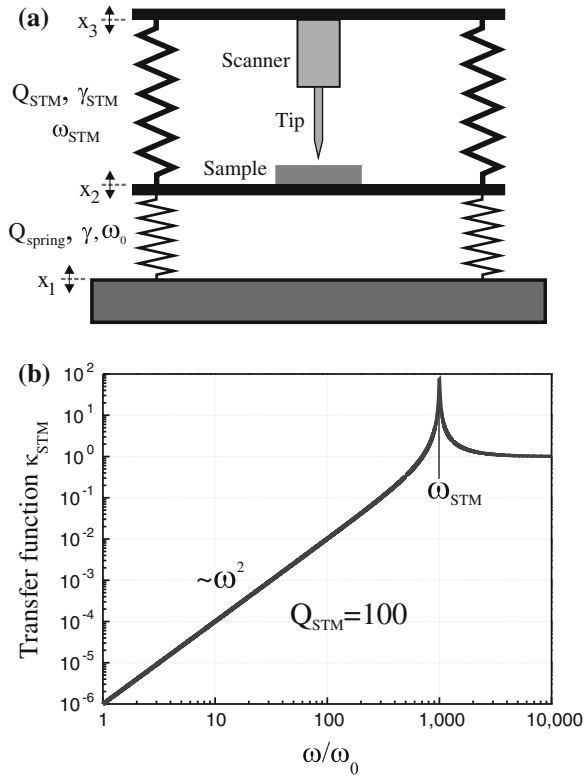
Note that the mass and the spring constant do not enter explicitly into the expression for the natural frequency. This equation is the same as for a simple pendulum with length Δl . Therefore, a spring suspension system acts as a isolation device for both vertical and horizontal environmental vibrations.

3.8.2 The Microscope Considered as a Vibrating System

In the second step of our analysis of the vibration isolation, we consider the microscope itself as a vibrating system. While it is wise to couple the sample most rigidly to the scanner/tip assembly, this (stiff) mechanical loop of the microscope can also be characterized as a vibrating system with a (quite high) resonance frequency ω_{STM} and a damping constant γ_{STM} , or corresponding quality factor $Q_{\text{STM}} = \omega_{\text{STM}}/\gamma_{\text{STM}}$ (Fig. 3.18). The softest part in the mechanical loop is the piezo material with a typical quality factor of 100. Let x_2 describe the oscillation of the microscope body (or sample in Fig. 3.18a), and x_3 the vibration of the scanner/tip assembly (Fig. 3.18a). Here one point is important (which makes life much easier): it is not the vibration amplitude of the tip x_3 (relative to the floor x_1) that has to be reduced to a minimum but only the *difference* of the motion between tip and sample $x_3 - x_2$. Only the relative motion of the tip relative to the sample counts! The differential equation for the vibrating tip x_3 relative to an external fixed reference is

$$\ddot{x}_3 + \gamma_{\text{STM}}(\dot{x}_3 - \dot{x}_2) + \omega_{\text{STM}}^2(x_3 - x_2) = 0. \quad (3.36)$$

Fig. 3.18 a The microscope itself is considered as an oscillating system characterized by ω_{STM} and γ_{STM} . Tip and sample oscillate against each other. **b** Transfer function κ_{STM} according to (3.40) for the microscope with resonance frequency ω_{STM}



The spring force is proportional to $x_3 - x_2$ and the frictional force is proportional to $\dot{x}_3 - \dot{x}_2$. Using the complex method to solve the differential equation results in

$$-\omega^2 x_3 + i\gamma_{STM}\omega(x_3 - x_2) + \omega_{STM}^2(x_3 - x_2) = 0, \quad (3.37)$$

or

$$-\omega^2 x_2 - \omega^2(x_3 - x_2) + i\gamma_{STM}\omega(x_3 - x_2) + \omega_{STM}^2(x_3 - x_2) = 0. \quad (3.38)$$

The (complex) ratio of the difference of the amplitudes $x_3^0 - x_2^0$ to the amplitude of the base of the microscope x_2^0 is obtained as

$$\frac{x_3^0 - x_2^0}{x_2^0} = \frac{\omega^2}{\omega_{STM}^2 - \omega^2 + i\gamma_{STM}\omega}. \quad (3.39)$$

The transfer function results in

$$\kappa_{STM}(\omega) = \left| \frac{x_3^0 - x_2^0}{x_2^0} \right| = \sqrt{\frac{\omega^4}{(\omega_{STM}^2 - \omega^2)^2 + \gamma_{STM}^2 \omega^2}}. \quad (3.40)$$

The resulting transfer function is plotted in Fig. 3.18b and can be approximated by

$$\kappa_{\text{STM}}(\omega) \approx \left(\frac{\omega}{\omega_{\text{STM}}} \right)^2, \quad (3.41)$$

for $\omega \ll \omega_{\text{STM}}$, and small damping, with ω_{STM} being the natural frequency of the STM (mechanical loop between tip and sample). When the excitation frequency ω is much lower than the natural frequency of the microscope ω_{STM} , good damping of the external vibrations is achieved. In Fig. 3.18b we use $Q_{\text{STM}} = 100$, since the material with the lowest Q -factor in the mechanical loop is the piezo ceramic, which has a typical mechanical quality factor of about 100.

3.8.3 Combining Vibration Isolation and a Microscope with High Resonance Frequency

The concept for an effective vibration isolation is to combine the two approaches and use a low natural frequency for the vibration isolation system and a high natural frequency for the mechanical loop of the microscope. According to (3.31), a vibration of the frame with amplitude $|x_1^0|$ is transmitted to the STM base with amplitude $|x_2^0|$ as

$$x_2^0 = \kappa_{\text{spring}} x_1^0. \quad (3.42)$$

(From now on, we consider the amplitudes as real and omit the absolute signs.) Furthermore the vibration amplitude of the STM base x_2^0 induces (according to (3.40)) a relative amplitude between tip and sample of

$$x_3^0 - x_2^0 = \kappa_{\text{STM}} x_2^0. \quad (3.43)$$

In total, an outer vibration of amplitude x_1^0 induces a relative tip sample vibration of amplitude $x_3^0 - x_2^0$ as

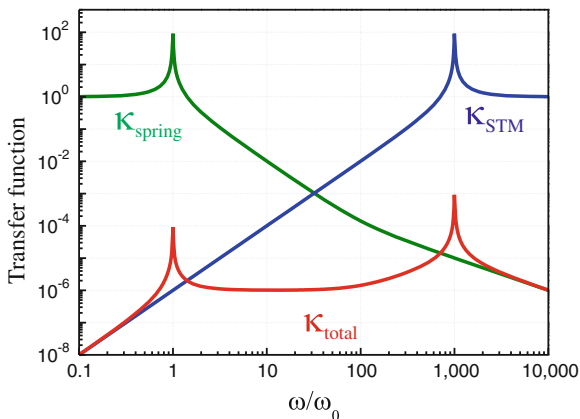
$$x_3^0 - x_2^0 = \kappa_{\text{STM}} x_2^0 = \kappa_{\text{STM}} \kappa_{\text{spring}} x_1^0. \quad (3.44)$$

or the total transfer function can be written as

$$\kappa_{\text{total}} = \frac{x_3^0 - x_2^0}{x_1^0} = \kappa_{\text{STM}} \kappa_{\text{spring}}. \quad (3.45)$$

The transfer function of the combined system is the product of the transfer functions of the individual systems.

Fig. 3.19 Transfer function of the combined system κ_{total} given by the product of the individual transfer functions of the spring suspension system κ_{spring} and the STM itself κ_{STM} for the case of small damping, i.e. $Q_{\text{STM}} = Q_{\text{spring}} = 100$



According to (3.34) and (3.41), the total transfer function can be approximated in the frequency range $\omega_0 < \omega < \omega_{\text{STM}}$ as

$$\kappa_{\text{total}} \approx \left(\frac{\omega_0}{\omega}\right)^2 \left(\frac{\omega}{\omega_{\text{STM}}}\right)^2 = \left(\frac{\omega_0}{\omega_{\text{STM}}}\right)^2. \quad (3.46)$$

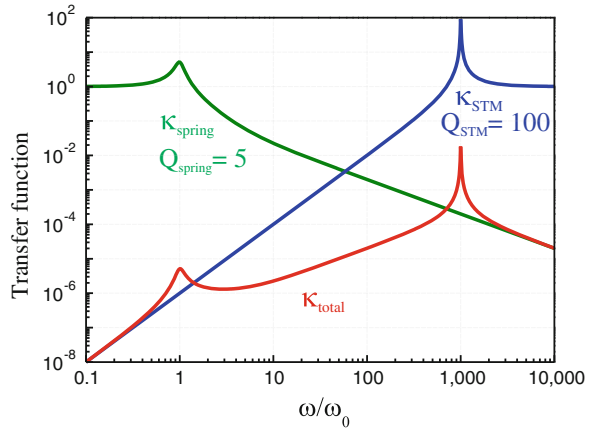
This behavior of an approximately constant transfer function in between the resonance frequencies ω_0 and ω_{STM} can be seen in Fig. 3.19 in which the transfer function is shown in the limit of negligible damping ($Q_{\text{STM}} = Q_{\text{spring}} = 100$).

If, for example, the natural frequency of the spring suspension system is 1 Hz and the natural frequency of the STM is 1 kHz, the overall transfer function for intermediate frequencies has a constant value of 10^{-6} , as shown in Fig. 3.19. If we would be able to raise the resonance frequency of the STM to 10 kHz the total transfer function for the transmission of an external vibration to the tip-sample distance would go to 10^{-8} !

Next we consider more realistic transfer functions by including damping. For the spring suspension system we consider $Q_{\text{spring}} = 5$, while we assume $Q_{\text{STM}} = 100$. When damping is included the total transfer function is not constant. The total transfer function according to (3.31) and (3.40) is plotted in Fig. 3.20 together with the individual transfer functions of the spring suspension and the STM. It is assumed that the STM mechanical loop can be approximated by a single natural frequency 1,000 times higher than the natural frequency of the spring suspension. With this assumption, the transfer function stays below the initial desired value of 10^{-5} up to $\omega/\omega_0 < 40$. The quite high values of the transfer function for higher frequencies (which arises due to the relatively strong damping of the spring suspension) could be regarded as problematic. However, as we will see in the next section, the driving amplitude of the exciting floor vibrations decreases at larger frequencies.

In summary, the spring suspension acts as a low-pass for vibrations with frequencies smaller than the natural frequencies of the spring ω_0 , while it damps the vibrations at larger frequencies. On the other hand, the STM assembly acts as a high-pass for

Fig. 3.20 Transfer function of the combined system κ_{total} which is the product of the individual transfer functions of the spring suspension system κ_{spring} and the STM itself κ_{STM}



vibrations with a frequency larger than ω_{STM} , while it damps the vibrations at lower frequencies. The total transfer function is the product of the transfer functions of the spring suspension and STM. In order to keep the total transfer function low at all frequencies, a low natural frequency of the vibration isolation, as well as a high frequency of the microscope mechanical loop are required.

The necessary damping of a spring suspension system is often performed by eddy-current damping. When a conductor (usually copper) moves in a magnetic field, damping forces are generated by eddy currents inside the conductor, as shown in the schematic in Fig. 3.21a. An example of an eddy-current damping system is

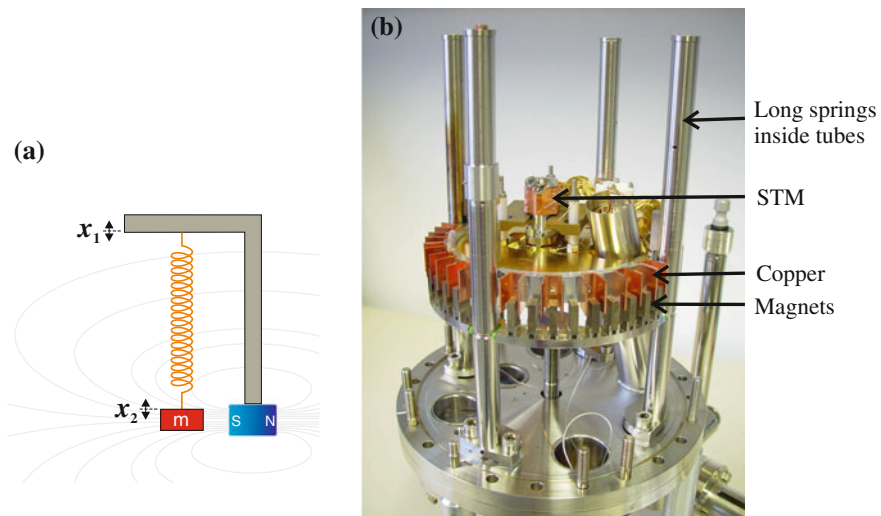


Fig. 3.21 **a** Principle of an eddy-current damping system with a magnet next to a conductor in which the energy is dissipated as eddy currents. **b** Photo of an eddy-current damping system with STM

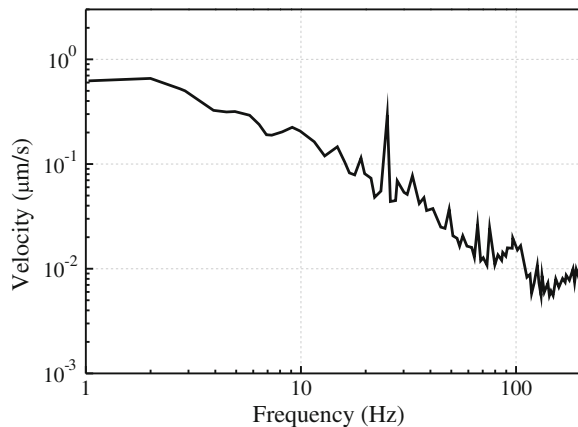
shown in Fig. 3.21b. The disadvantage of a spring suspension system is the large size. Another way of damping is to use a stack of metal plates separated by rubber (e.g. Viton[®]) pieces, which act as springs and dampers simultaneously. A further method of vibration isolation is to mount the SPM on pneumatic isolation legs (also used for optical tables). A typical resonance frequency of such a table is 1–2 Hz, and a transfer function of smaller than 0.01 can be achieved for frequencies larger than 10 Hz.

3.9 Building Vibrations

Building vibrations are most pronounced in the low frequency range below 10 Hz. Building vibrations can be influenced by external conditions like nearby railway lines or motorways. Also inside a building the building vibrations are increased by compressors, large machines, and ventilation systems. As a general rule the intrinsic building vibrations are more pronounced in higher floors and correspondingly lowest in the basement of a building. For this reason, sensitive scanning probe microscopes can be often found in the basement.

Geophones (accelerometers) are typically used to measure building vibrations. The quantity measured by these instruments is the velocity. In Fig. 3.22, the velocity of the building vibrations measured on a floor in a building in Research Center Jülich is plotted as function of vibration frequency. The general behavior is that the amplitude decreases with increasing frequency. The highest amplitudes are typically observed for low frequencies around 1–2 Hz. In Fig. 3.22 a value of $v_0 \approx 0.7 \mu\text{m/s}$ is observed at low frequencies. In order to convert the measured data from the velocity to oscillation amplitude or acceleration, we recall that

Fig. 3.22 Velocity of the building vibrations measured on the floor in a building at the Research Center in Jülich



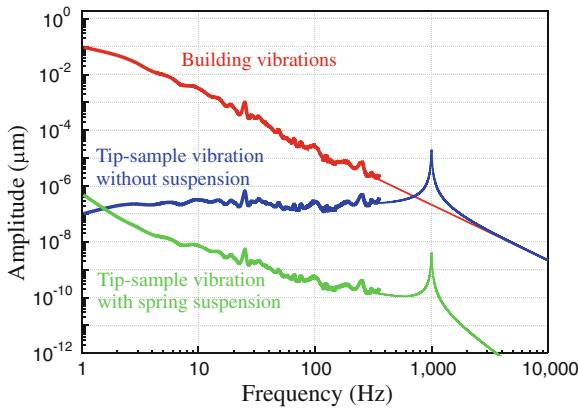


Fig. 3.23 Expected tip-sample vibrational amplitude as a function of frequency, calculated using the measured building vibrations and the appropriate transfer function from Fig. 3.20. The amplitude of the building vibrations is shown as a *red line*. The data are taken from Fig. 3.22 and extrapolated for higher frequencies. The *green* and *blue curves* show the behavior with and without a spring suspension system, respectively

$$x = x_0 \cos(\omega t), \quad (3.47)$$

$$v = \dot{x} = -x_0 \omega \sin(\omega t) := -v_0 \sin(\omega t), \quad (3.48)$$

$$a = \ddot{x} = -x_0 \omega^2 \cos(\omega t). \quad (3.49)$$

Therefore, the vibration amplitude at 2 Hz is $x_0 = v_0/\omega \approx 50$ nm. The corresponding acceleration is $a_0 = \omega v_0 \approx 10^{-5}$ m/s² ≈ 1 μ g.⁴

The measured building vibrations $x_1^0(\omega)$ can be included in the vibration analysis performed previously. According to (3.44), the relevant tip-sample vibrational amplitude $x_3^0 - x_2^0$ can be expressed as a function of frequency as

$$x_3^0 - x_2^0 = \kappa_{\text{total}}(\omega)x_1^0(\omega). \quad (3.50)$$

If we multiply the total transfer function by the measured floor vibration amplitude (derived from Fig. 3.22), the expected tip-sample vibration amplitude arising due to the floor vibrations is shown in Fig. 3.23. The case where no spring suspension is invoked is shown as blue line, leading to a roughly constant tip-sample vibration amplitude of 10^{-4} nm = 0.1 pm. However, close to the resonance frequency of the STM the amplitude increases by the usually quite high quality factor of the STM. This disadvantageous resonance behavior (amplitude up to 0.1 nm) can be suppressed using a spring suspension system. The tip-sample vibrational amplitude including a spring suspension (green curve) suppresses the amplitude at STM resonance

⁴ Sometimes a factor of $1/\sqrt{2}$ is included if the root mean square (RMS) amplitude instead of the peak amplitude is measured.

frequency, but also leads to a resonance at the eigenfrequency of the spring suspension system, which has to be suppressed by proper damping of the spring suspension system. In this case, the tip-sample vibrations are reduced to values below one picometer for all frequencies.

3.10 Summary

- Due to the piezoelectric effect a voltage applied to the electrodes of a piezoelectric element leads to a strain, i.e. a motion of some part of the element.
- The piezo constant describes the sensitivity of a piezoelectric actuator in $\text{\AA}/\text{V}$.
- The most frequently used piezoelectric actuator element in scanning probe microscopy is the tube piezo element. It allows x , y , and z -motion with one single element.
- Problems with piezoelectric actuators are the coupling of lateral and vertical motion, non-linearity, hysteresis, and creep.
- Sharp STM tips can be fabricated by self-adjusting electrochemical etching.
- The natural frequency of a spring suspension system depends only on the extension length Δl as $\omega_0 = \sqrt{\frac{g}{\Delta l}}$.
- It is not necessary to minimize the amplitude of the tip vibration and the sample vibration individually but only the *difference* between tip and sample position.
- For effective vibration isolation a low natural frequency of the spring suspension system ω_0 is combined with a high natural frequency of the STM assembly ω_{STM} , i.e. a stiff mechanical loop between tip and sample.
- The transfer function (i.e. the attenuation of external vibrations) is constant for small damping $\kappa_{\text{total}} \approx (\frac{\omega_0}{\omega_{\text{STM}}})^2$ for $\omega_0 < \omega < \omega_{\text{STM}}$.
- The expected tip-sample vibration amplitude can be calculated by multiplying the total transfer function by the (measured) building vibration amplitude.